*J. Fluid Mech.* (1969), *vol.* 36, *part* 3, *pp.* 447–464
*Printed in Great Britain*



# An experimental investigation of disturbance amplification in external laminar natural convection flow

By R. P. DRING
N.S.F. Trainee, Cornell University

AND B. GEBHART
Professor of Mechanical Engineering, Cornell University

(Received 15 May 1968)

An experimental investigation has been carried out on the nature of disturbance amplification in the laminar natural convection boundary layer formed on a vertical flat surface with uniform heat flux input. A pair of calibrated hot-wire anemometers were used to obtain amplitude and phase profiles of disturbance velocities and to measure the distance amplification rate as a function of disturbance frequency. An interferometer was used to measure the amplitude and phase profiles of disturbances in the temperature field. The relative amplification of a temperature disturbance was measured as it was convected downstream. For this latter measurement a technique employing interferometric *moiré* patterns was used. All of these measurements are in good agreement with the theory. The results of this investigation further strengthen the conclusions drawn in an earlier theoretical investigation, that the frequencies which amplify fastest and lead to transition and turbulence occupy a band much higher than the frequencies which begin to amplify first. These results also support stability theory in the very close agreement between calculated and measured distributions of disturbance quantities.

## 1. Introduction

The theoretical results of Dring & Gebhart (1968) predict how disturbances are modified as they are convected downstream in a uniform surface heat flux natural convection boundary layer on a vertical surface. The coupled Orr–Sommerfeld equation was numerically integrated for a Prandtl number of 6·7. Spatial amplification rate contours were located and amplitude ratio contours were determined from them. From these results, it was seen that the low-frequency disturbances (of very long wavelengths), which are predicted to be unstable first, amplify very slowly. There was seen to be a band of higher-frequency (shorter wavelength) disturbances which amplify much faster. These will perhaps turn out to be the dominant ones in instability and transition considerations. The nature of the velocity and temperature amplitudes and phase

profiles was also examined. The object of the experimental investigation was to compare the theoretical disturbance profiles and growth rates with measured behaviour. The entire investigation was carried out in the amplified region of the stability plane.

Schubauer & Skramstad (1948) conducted an investigation for the Blasius profile which is in many ways similar to the present work. They initiated oscillations in the boundary layer with a vibrating ribbon and measured disturbance profiles and amplification. Their work verified many of the theoretical predictions for the neutral curve and for the amplification rates of the Blasius profile. Some of the measurement techniques employed by these authors were applied to the natural convection profile in the present work.

Colak-Antic (1964) reported some hot-wire investigations of disturbances in the natural convection flow of air over a large (2 m × 1 m) vertical isothermal surface. Disturbances were introduced by pulsing the electrical input to a heater wire in the boundary layer. No mention was made of how far downstream the effects of this disturbance generator were found in the base flow profiles. The relatively high temperature differences involved in these studies (about 20 °F) made calibration of the anemometer difficult. Influences of both the local temperature and flow velocity were coupled in the anemometer output. Since, in air, the velocity and temperature boundary layers are approximately of the same thickness, there is a first-order temperature coupling. As a result, much of this work is qualitative in nature.

Polymeropoulos (1966) performed the first critical experimental study of instabilities in natural convection flows. A 20 cm Mach–Zehnder interferometer was used to investigate neutral stability for the flow over a vertical uniform flux surface in pressurized nitrogen. A vibrating ribbon in the boundary layer produced the disturbances. The principal results in Polymeropoulos & Gebhart (1968) are in good agreement with Nachtsheim's (1963) numerical solutions of the coupled Orr–Sommerfeld equation for a natural convection boundary layer and with the calculation of Polymeropoulos & Gebhart (1966) for uncoupled disturbances in the flow induced by a uniform flux boundary condition.

Knowles (1967) refined the equipment and procedures used by Polymeropoulos (1966) and applied them to the natural convection flow of a liquid (having a high Prandtl number) over a vertical, electrically heated, uniform flux surface. In addition to interferometric studies of the disturbances in the temperature field, the behaviour of velocity disturbances was investigated with a hot-wire anemometer. There was little temperature coupling in the anemometer output due to the low-temperature excesses used and the relatively thin thermal boundary layer (relative to the velocity boundary-layer thickness). The experimental data were in good agreement with the theoretical results in predicting the location of the neutral curve. From this work it was apparent that the frequency of a disturbance remains constant as it is convected downstream, suggesting that the disturbance frequency is a better basis on which to investigate stability than is wave-number. The wave-number is more difficult to measure and changes as a disturbance is convected along.

## 2. Apparatus

The thermal boundary layer has been examined with a 20 cm Mach–Zehnder interferometer and the velocity boundary layer has been investigated with a pair of constant-temperature hot-wire anemometers. Many of the techniques used to measure disturbance amplitude and phase profiles, and amplification, in the temperature field in the present work are identical with those employed by Polymeropoulos & Gebhart (1968) and by Knowles (1967). Both of these studies and part of the present work were carried out on the interferometer described by Gebhart & Knowles (1966). The hot-wire anemometers, and their related equipment, had also been used by Knowles (1967).

The test liquid used was a silicone fluid (hexamethyldisiloxane). It is similar to water in many respects and it has a nominal viscosity of 0·65 cst. This particular fluid was chosen for several reasons. Temperature differences on the order of a fraction of a degree give Grashof numbers in the range desired for the length of the vertical surface visible in the interferometer. Because of its relatively high Prandtl number (6·7), the thermal boundary layer is considerably thinner than the velocity boundary layer. These low temperatures and their narrow range of influence greatly simplified the anemometry by eliminating the effect of temperature coupling on the hot-wire output. At the resistance ratio used (i.e. the ratio of the probe resistance at its working temperature to that at room temperature, 1·3) the probe sensor temperature excess (approximately 115 °F) was much greater than the variation of the fluid temperature across the boundary layer (approximately 0·6 °F). A Prandtl number in this range was also desirable from the standpoint of the theory since solutions (by Knowles & Gebhart 1968) had only been determined up to a Prandtl number of 6·9.

The heated vertical surface was a sheet of Inconel-600 foil (0·0005 in. thick, 2·00 in. wide and 12·72 in. long). The foil was heated by passing a current through it. In this work, a current of one ampere was used. The measured foil resistance was 0·484 ohms. The foil was stretched between a pair of knife edges. The lower knife edge can be seen in the interferograms (figures 5 and 7), expanded horizontally by the anamorphic lens system used.

The vibrator used to introduce disturbances into the boundary layer was a strip of metal foil (0·005 in. thick, $\frac{1}{8}$ in. high and 6 in. wide). It was mounted horizontally in the boundary layer and $1\frac{1}{2}$ in. from the leading edge. The strip was mounted on the open ends of a V-shaped support. The support was driven by an electromagnet. The amplitude and frequency of the input to the vibrator were controlled by a function generator and could be set over a wide range. The vibrator amplitude was always very small relative to the boundary-layer thickness.

The vertical foil and the vibrator assembly were mounted on a positioning apparatus. It permitted a precise alignment of the foil in the interferometer beam. A grid of horizontal wires was added to indicate location. The first wire was at the leading edge and the second was $\frac{1}{2}$ in. above. The rest were at 1 in. intervals up to $6\frac{1}{2}$ in. These wires can be seen in the interferograms.

The positioning apparatus (and all of the equipment attached to it) was

mounted in the test vessel of the interferometer. Two hot-wire anemometer probes were mounted on another positioning apparatus which was connected to the lid of the test tank. Each probe was mounted on an independent traversing mechanism and could be positioned vertically to an accuracy of 0·010 in. by means of scales cemented to vertical slide columns. They could be positioned normal to the foil to an accuracy of less than 0·001 in. by micrometer-driven traverses. The probes point upstream (i.e. downward) into the rising natural convection flows. This is the configuration under which they had been calibrated, i.e. the fluid rising past a stationary probe. The calibration of the anemometers is described in appendix A. The anemometer was measured either with a digital voltmeter (for time-steady measurements) or with a pen recorder (for unsteady measurements).

The construction and operation of the interferometer are described in detail by Gebhart & Knowles (1966). The output beam passes through two cylindrical lenses. These lenses compress the beam vertically from an aspect ratio of 8 : 1 to 5 : 4. The isotherms in the thermal boundary layer appear as fringe shifting in the interferometer. The compression of the vertical direction by the cylindrical lenses greatly improves the resolution of these fringes. This is the reason for the unusually thick appearance of the thermal boundary layer in the interferograms.

The various components of the apparatus are described in greater detail by Polymeropoulos (1966), Knowles (1967) and Dring (1968).

## 3. Measurements

*Disturbance velocity profiles*

Disturbance velocity amplitude and phase profiles were measured at four locations along the foil. Measurements were made at $x = 2$ in., $3\frac{1}{2}$ in., 5 in. and $6\frac{1}{2}$ in., and at a disturbance frequency $f$ of 0·2 Hz. This is close to the highest frequency which is in the amplified region over the entire test range (from the vibrator at $x = 1\frac{1}{2}$ in. to $x = 6\frac{1}{2}$ in.). A high frequency was desired in order to minimize the test time. For profiles at each location, both hot-wire probes were placed at the same distance from the leading edge $x$ at different span-wise locations. One probe was left stationary as a phase reference and as an indicator of any time variation in the disturbances. This probe was located in the boundary region near the experimentally determined disturbance amplitude maximum and its output was recorded. The other probe was traversed across the boundary layer (at constant $x$). It was stopped at each of seventeen locations long enough for several cycles to be registered on the pen recorder at each location. The amplitudes at the various locations were normalized with respect to the maximum in the traverse and the local phase was measured relative to that of the stationary probe.

Several boundary-layer traverses were made at each location to give an estimate of the error to be expected. Only two traverses are shown (in figure 1 at $x = 2$ in. and in figure 2 at $x = 6\frac{1}{2}$ in.) at each location. In the figures, $\eta = y/\delta_c$, where $y$ is the distance normal to the surface and $\delta_c = 5x/G^*$. The parameter $G^*$ is defined as $5(Gr^*/5)^{\frac{1}{5}}$, where $Gr^* = g\beta_T q'' x^4/k\nu^2$ is the flux Grashof number, $g$ is the acceleration of gravity, $\beta_T$ is the coefficient of thermal expansion, $q''$ is the

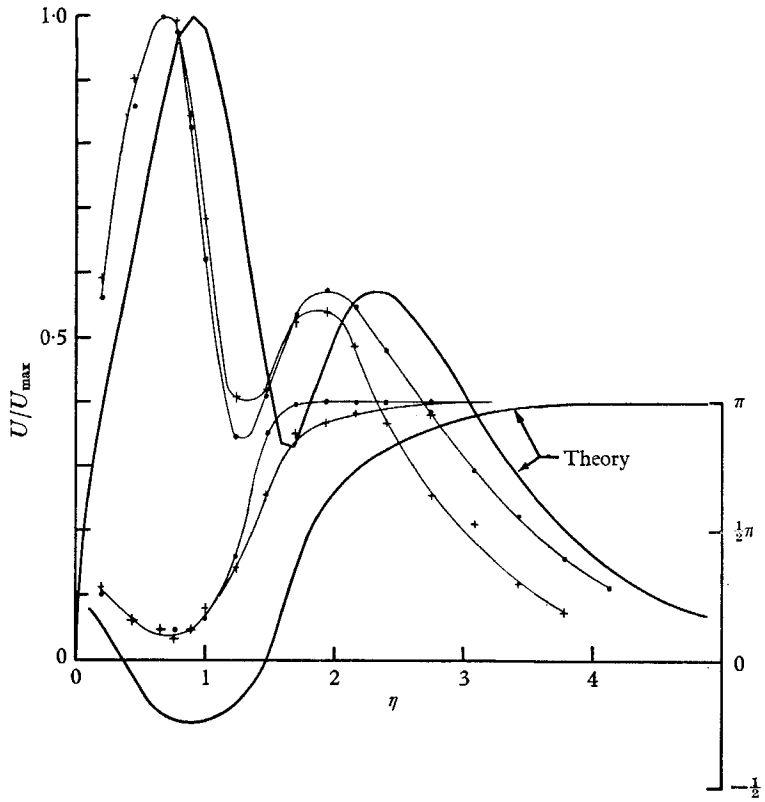


FIGURE 1. The disturbance velocity profile at $x = 2$ in., $f = 0{\cdot}2$ Hz, $G^* = 115{\cdot}5$. Theory: $G^* = 100$.

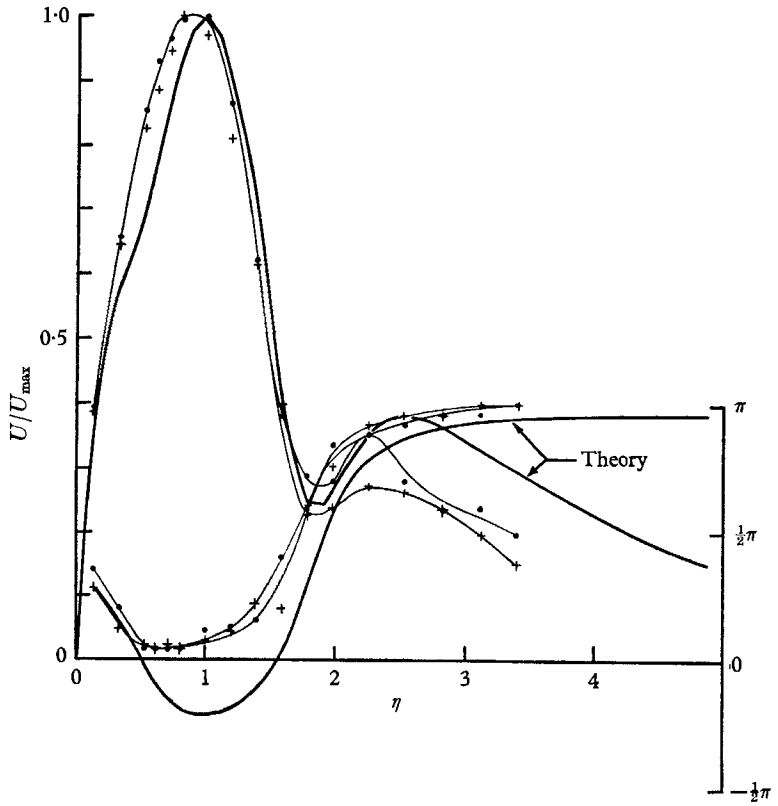


FIGURE 2. The disturbance velocity profile at $x = 6\frac{1}{2}$ in., $f = 0{\cdot}2$ Hz, $G^* = 296{\cdot}5$. Theory: $G^* = 300$.

heat flux, $x$ is the distance from the leading edge and $k$ and $\nu$ are the thermal conductivity and kinematic viscosity respectively. These traverses are indicative of the spread in the results. The amplitudes have not been corrected to account for the slope variation of the calibration curve (figure 11). At $\eta = 4$ this correction would increase the disturbance amplitude by about 35 %. In the region far from the surface where these corrections become significant (i.e. where flow speed is

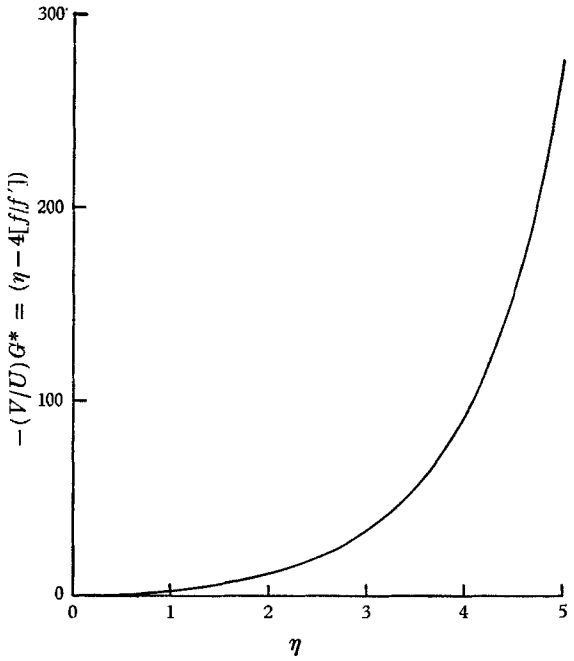


FIGURE 3. $-(V/U)G^*$ *versus* $\eta$.

very low) the base flow is no longer vertical. The normal and tangential velocity components (i.e. $V$ and $U$ respectively) are compared in figure 3. They are of the same order of magnitude near the edge of the boundary region. Since the calibrations were conducted for a purely vertical flow, they are not accurate here.

Only the measured disturbance velocity profiles at 2 in. and $6\frac{1}{2}$ in. are shown. Changes in the amplitude and phase profiles of a disturbance as it is convected downstream are not great, but they can be seen at these two locations (figures 1 and 2). The two most obvious changes in the theoretical and measured profiles are the broadening of the amplitude maximum near the foil and the reduction in the relative size of the smaller maximum. At the foil current of 1 A the curve $f_3$ in figures 1 and 2 of Dring & Gebhart (1968), and in figure 10 of the present work, corresponds to a frequency of 0·2 Hz, i.e. the experimental value. The two sets of theoretical profiles in figures 1 and 2 are taken near $f_3$, at $G^* = 100$ and at $G^* = 300$. At 1 A, the 2 in. location corresponds to $G^* = 115{\cdot}5$ and $6\frac{1}{2}$ in. corresponds to $G^* = 296{\cdot}5$.

There are, however, some significant differences between the theoretical and experimental results. The phase shift across the boundary region predicted by

the theory is about 225°. This is generally about 27 % greater than that found by experiment (about 170°). All of the major characteristics of the theoretical results can be seen in the experimental data. There is some general disagreement in profile shape.

*Amplification rate from velocity measurements*

The distance amplification rate was measured from the disturbance velocity amplitude growth. The method employed is similar to that used by Schubauer & Skramstad (1948). Their comparable results are summarized in figure 28 of their work. The disturbance velocity amplitude was measured at two different distances from the leading edge (namely at $3\frac{1}{2}$ in. and 4 in.). From the ratio of the amplitudes at these two locations the amplification rate was determined.

To compare the measurements reported here with theory, the approximation is made in equation (12) of Dring & Gebhart (1968) that the non-dimensionalized spatial amplification rate $\alpha_i$ is constant from $G_1^*$ to $G_2^*$. The error involved in this approximation is relatively small for the values of $G^*$ used. The variation is also small relative to the spread in the experimental results. This approximation leads to the following expression:

$$\alpha_i = (-4/[G_2^* - G_1^*]) \ln (A_2/A_1), \tag{1}$$

where $A_2/A_1$ is the non-dimensionalized disturbance amplitude ratio for the two locations. The velocities were non-dimensionalized with a characteristic convection velocity ($U_c = \nu G^{*2}/5x$), which is proportional to $x^{\frac{3}{5}}$. Thus we have

$$A_2/A_1 = (U_2/U_1)(x_1/x_2)^{\frac{3}{5}}, \tag{2}$$

where $U$ and $x$ are the physical (dimensional) values. Combining these relations and using the values of $x_1 = 3\frac{1}{2}$ in. and $x_2 = 4$ in., we get

$$\alpha_i = (-0{\cdot}1966) \ln [0{\cdot}9231(U_2/U_1)]. \tag{3}$$

The ratio $U_2/U_1$ was determined by measuring the maximum amplitude of the anemometer disturbance output at each location. One probe was located at $3\frac{3}{4}$ in. from the leading edge and at a distance normal to the foil that would correspond to the experimental disturbance amplitude maximum. This gave a record of the time history of the disturbance amplitude at that location. The second probe was used to traverse the boundary layer. Amplitudes were recorded at four or five locations near the maximum amplitude at $x = 3\frac{1}{2}$ in. and then the same probe was moved to $x = 4$ in., where another traverse was made. The same probe was used at both locations to eliminate the need for corrections based on different sensitivities of the two anemometers. This method is superior to that used by Schubauer & Skramstad (1948) because in the present work the boundary layer was traversed at each location to determine the disturbance amplitude maximum. In their work the same normal distance was used at both locations.

The ratio of the maximum disturbance amplitudes of the anemometer output at the two locations was taken as the ratio of the dimensional disturbance velocity amplitudes $U_2/U_1$. The correction to the anemometer sensitivity due to the slight increase in base flow velocity (a few percent) was ignored. This correction would have accounted for the slightly different slopes of the calibration curve at the two base flow velocity levels.

The non-dimensionalized amplification rate $\alpha_i$ was measured at four different frequencies. Measurements were repeated several times at each frequency to give an indication of the error in the measurements. The experimental and theoretical results were compared on a plot of $\alpha_i$ *versus* $\beta$ (the non-dimensionalized frequency) in figure 4. The theory results are for $G^* = 191$, which corresponds to $x = 3\frac{3}{4}$ in. (i.e. the mean location). The non-dimensionalized frequency $\beta$ was calculated from the physical frequency $f$ and from the characteristic velocity $U_c$ and length $\delta_c$ evaluated at $3\frac{3}{4}$ in. The result is

$$\beta = 2\pi(\delta_c/U_c)f = 0{\cdot}3272f \text{ Hz}. \tag{4}$$

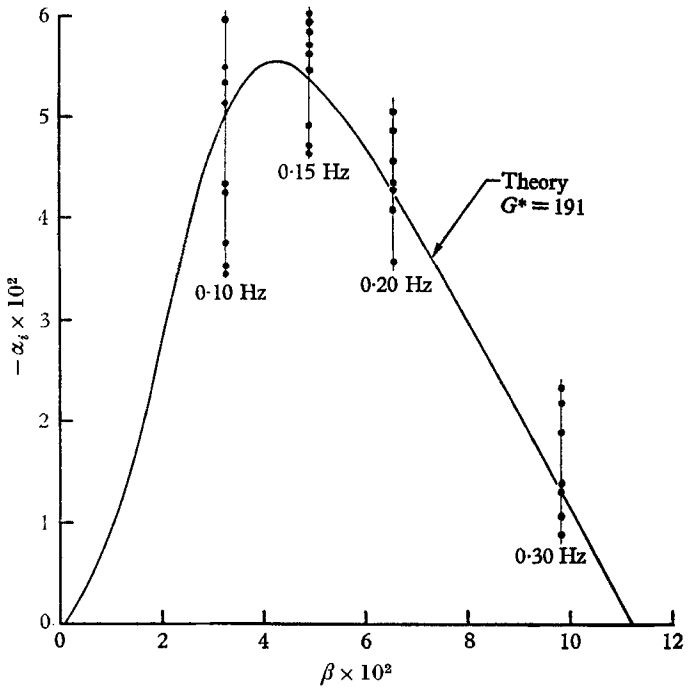


FIGURE 4. An experimental and theoretical plot of $-\alpha_i$ *versus* $\beta$ at $G^* = 191$.

In his investigations of the neutral curve, Knowles (1967) shows scatter in his experimental results at this $G^*$ to be from $\beta = 0{\cdot}105$ to $0{\cdot}120$ (refer to figure 53 of that work). This corresponds well with the uncertainty of the results presented here if the band of uncertainty is extrapolated to $\alpha_i = 0$ at large $\beta$.

For the low-frequency range, i.e. less than 0·1 Hz, it was found that the waves were not a single, pure sinusoid. At these frequencies higher harmonics tended to dominate the disturbances. If a frequency of 0·06 Hz was introduced, the dominant disturbance frequency in the fluid appeared to be 0·12 Hz. This phenomenon is discussed in detail in a later section of this paper. Since a 'pure' disturbance, i.e. a disturbance with only one frequency present and no higher harmonics, could not be produced at frequencies less than 0·1 Hz, the amplification rate could not be measured in this range. These higher harmonics are also believed to be the reason for the relatively large spread in the results at 0·1 Hz in figure 4.

*Disturbance temperature profiles*

An infinite fringe adjustment on the interferometer was used in the measurement of the amplitude and phase profiles of the disturbance temperature. The frequency used in this measurement was also 0·2 Hz, as in the measurement of the

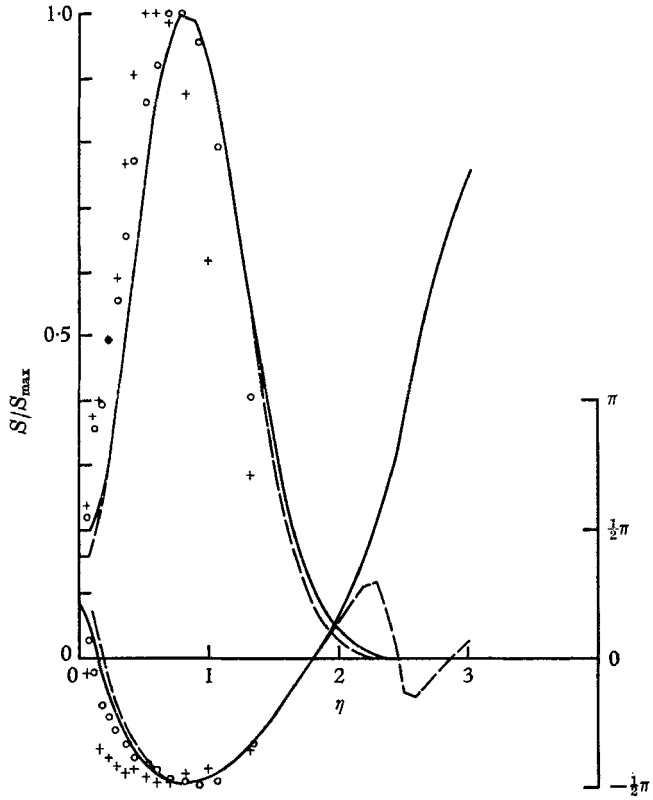


FIGURE 6. The disturbance temperature profiles. Data: $f = 0{\cdot}2$ Hz; +, $G^* = 159{\cdot}8$, $x = 3$ in.; ○, $G^* = 278{\cdot}2$, $x = 6$ in. Theory: $f_3$: ——, $G^* = 150$; — — —, $G^* = 300$.

disturbance velocity profiles. At a current of 1 A, this frequency is represented by curve $f_3$ in figure 10 and in the $\beta/G^*$ diagrams of Dring & Gebhart (1968) (figures 1 and 2 of that reference). The technique used here is essentially the same as that discussed by Knowles (1967), i.e. the temperature disturbance amplitude is equal to the fringe displacement amplitude divided by the fringe spacing.

Measurements were taken from the interferogram (figure 5, plate 1) with an optical comparator. There is a variation of about half a fringe in the far field of this interferogram. The location normal to the foil was scaled from the location of the hot-wire probe seen to the left of the boundary layer, 2 in. from the leading edge, 0·300 in. from the foil. All normal distances were scaled from this. The horizontal grid wires provided scaling for distances parallel to the foil. Along each fringe, two wave maxima and two wave minima were located around the station (in $x$) at which the profile was to be measured. One maximum and one

minimum were above the station and one of each was below. By interpolation the fringe amplitude and mean position could be located for each fringe at the station. A base flow temperature profile was plotted (i.e. fringes *versus* normal distance) using the mean fringe positions. The temperature amplitude profile was determined by plotting the fringe displacement amplitudes about their mean positions and projecting them to the ordinate (i.e. the fringe co-ordinate). Since the temperature change is proportional to the fringe shift, this gives the temperature amplitude profile. The temperature amplitude of each fringe is plotted at the mean position of that fringe (figure 6). Also shown in this figure is the phase profile. This was taken directly from the longitudinal $x$ location of the fringe maxima. Each fringe is represented on the amplitude and phase profiles by a point on each curve. This process was repeated twice, once at 3 in. ($G^* = 159{\cdot}8$) and once at 6 in. ($G^* = 278{\cdot}2$). Comparisons with theory are shown in figure 6.

The experimental amplitude maxima are located slightly nearer to the surface than the single theoretical one. This trend can be seen in the entire amplitude profile as well as in the phase profile. The experimental profiles are slightly narrower than the theoretical profiles. In figures 1 and 2 we saw the same general result. The experimental disturbance velocity profiles are narrower than the theoretical ones.

All of the experimental results of the present work are compared with the theoretical results of Dring & Gebhart (1968), in which the disturbance heat flux $s'$ was assumed to be zero at the surface. In the stability theory results for this flow (i.e. Knowles & Gebhart (1968) and Dring & Gebhart (1968)), the proper thermal boundary condition was shown to be that a linear combination of the disturbance temperature $s$ and disturbance flux $s'$ be zero at the surface. At low values of $G^*$ this boundary condition approaches the $s'(0) = 0$ case. At large values of $G^*$ it approaches the $s(0) = 0$ case. For computational simplicity and because of the relatively low values of $G^*$ being considered, the $s'(0) = 0$ boundary condition was used for all theory calculations.

The theoretical results, with $s'(0) = 0$, figure 6, show that $s(0)/s_{\max} = 0{\cdot}197$ at $G^* = 150$ and $0{\cdot}159$ at 300 for a disturbance frequency of 0·2 Hz, i.e. $f_3$. The plotted experimental results neither support nor cast doubt on the validity of this boundary condition. The last fringe, i.e. the fringe nearest to the foil, whose maxima and minima could be clearly seen was too far from the foil to shed any light on this question. There was one additional fringe immediately next to the foil. Although amplitude measurements could not be taken from it, it indicates that the $s'(0) = 0$ boundary condition is not yet completely accurate (although it will become so at larger values of $G^*$).

### *Amplification of temperature disturbances*

Temperature disturbances may amplify as they are convected downstream. This can be seen in the temperature field as the increasing of a disturbance amplitude along an isotherm. This is seen in an interferogram as the increase in the disturbance amplitude along a fringe with distance from the leading edge (see figure 5, plate 1).

In this investigation it is necessary that the disturbance amplitudes be

measured along an isotherm and the interferometer, with the infinite fringe adjustment, is a convenient instrument in that it provides visual evidence of the isotherms (i.e. the fringes). The fringes, however, can only be taken as isotherms if a good infinite fringe can be achieved in the distant field. The fringes are lines of constant optical path length. They correspond to isotherms only if there are no fringes in the undisturbed region far from the foil. With the 27 in. optical path length through the fluid in the test tank and in the compensating tank, a temperature difference of 0·004 °F in the fluid can cause a fringe to appear. Since it is almost impossible to reach such a high degree of uniformity of the fluid temperature, it was very rare that a good infinite fringe adjustment could be achieved.

A finite fringe technique was used in order to avoid this difficulty. The interferometer was adjusted to have a vertical density of horizontal fringes about 10–12 fringes per inch. When the foil was heated the fringes were displaced. Pictures were taken by a double exposure method. A sheet of film was exposed once before the foil was heated and once again at the experimental conditions. A *moiré* pattern results (e.g. figure 7, plate 2). The *moiré* fringe field is purely a result of the temperature field about the vertical foil. This fringe pattern does truly represent the isotherms. This method gives an accurate representation of the isotherms regardless of what the initial temperature field may have been. This is a pseudo-infinite fringe technique of great utility in difficult circumstances.

The isotherm pattern is seen in the *moiré* pattern. The overlapping of the displaced and undisplaced fringes has caused dots where the fringes were displaced by one fringe spacing and grey areas where they were displaced by half a spacing. The isotherms are contours of constant fringe difference.

Inaccuracy can arise if there is a shift in part, or all, of the background field. If the temperature along a light path through the fluid far from the foil changes by 0·004 °F, this will cause a displacement of one fringe along that path. Thus very slight temperature changes in the bulk of the fluid between the two exposures will distort the pattern (i.e. the fringes will no longer represent isotherms). Recall that the *moiré* pattern is a result of the changes in the optical path length field between the two exposures. The time lapse between the two exposures was about 3–4 min. This time was required to get a steady base flow (from an initially quiescent fluid), to start the vibrator and for the disturbances to reach steady state. Steady state in the base flow and in the disturbances was indicated by the output of the anemometer seen near the top of the optical field (at $x = 6\frac{1}{2}$ in.). Data were not taken if the fringe pattern was not sharp in the region far from the foil, i.e. if there had been a fringe shift in this region. It was very difficult to get interferograms entirely free of some shift, but in many cases the effect was very small. Although the fringe shift patterns are not as distinct by this method as they are with an infinite fringe adjustment (e.g. figure 5, plate 1) they are usually more accurately representative of the isotherm pattern about the heated foil.

The fringe displacement amplitudes were measured along the fringe that corresponded most closely, over a variation in $x$, to the experimental disturbance temperature maximum, i.e. the fifth fringe in from the undisturbed region far from the foil. This can be seen in the infinite fringe interferogram (figure 5, plate 1) and in the disturbance temperature amplitude and phase profiles taken from it

(figure 6). Each fringe in figure 5 is represented by a point in both the amplitude and phase profiles of figure 6. The maximum in the amplitude profile corresponds most closely to the fifth fringe in from the undisturbed far field. The experimental results plotted in figure 8 as dashed curves were obtained by measuring the loca-

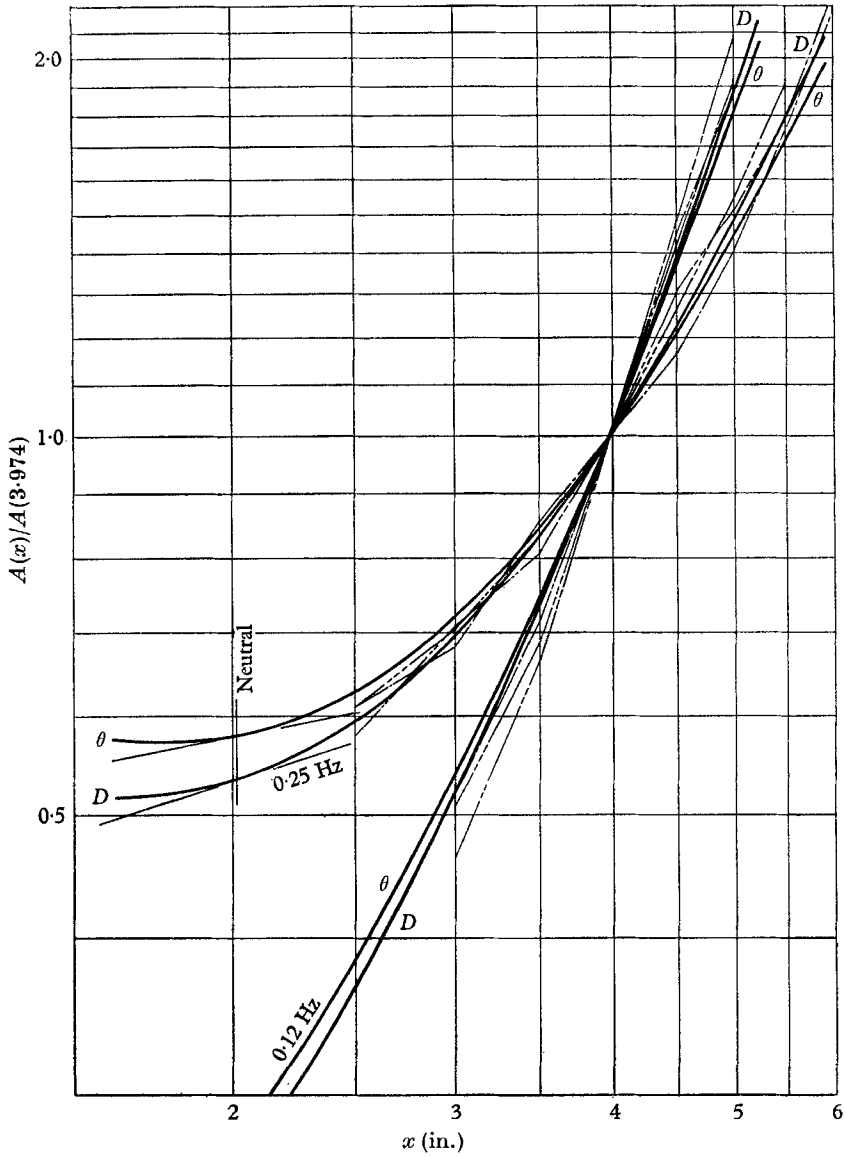


FIGURE 8. Amplification of disturbance temperature at 0·12 Hz and 0·25 Hz. ——, theory: – – – –, experimental results.

tions of the maxima and minima along this fringe. Measurements were made on an optical comparator. The horizontal grid wires provide vertical scaling. The location of each maximum and minimum, i.e. the location parallel to and normal to the foil, was plotted, and the maxima and minima were fitted with two curves

which defined an envelope for the fringe. The amplitudes, i.e. the envelope widths, were then measured at various locations relative to the amplitude at $x = 3{\cdot}974$ in. ($G^* = 200$).

The data were given a slight correction based on the time history of the disturbance amplitude as indicated by the anemometer at $x = 6\frac{1}{2}$ in. This was done by marking the time of the second exposure on the recorder tape. This permitted the disturbances in an interferogram to be synchronized with the recording. The amplitudes of the disturbances measured on the photograph were corrected based on the amplitudes they had as they passed the anemometer probe. This correction was always small (less than 5 %) relative to the scatter in the results.

The total disturbance amplification may perhaps be looked at as the sum of two separate mechanisms. The base flow quantities are increasing in the downstream direction and disturbances might grow proportionately. For temperature disturbances, this type of growth is proportional to the $x^{\frac{1}{4}}$ (or $G^{*\frac{1}{4}}$) growth of the characteristic temperature, $T_c = 5q''x/kG^*$. The second mechanism of disturbance growth is characterized by the Orr–Sommerfeld equation. It predicts the decay or growth of the non-dimensionalized disturbances. The relative growth due to the combined mechanisms was calculated by this means and normalized to one at $G^* = 200$ (i.e. at $x = 3{\cdot}974$ in.). This results in the following expression:

$$\theta_{G^*}/\theta_{200} = (G^*/200)^{\frac{1}{4}} \exp\left(-\frac{1}{4}\int_{200}^{G^*} \alpha_i \, dG^*\right), \tag{5}$$

where $\theta_{G^*}/\theta_{200}$ is the ratio of the dimensional disturbance temperature amplitude at some $G^*$ to that at $G^* = 200$. The fourth root of $G^*$ is the dimensional characteristic temperature growth and the exponential is the non-dimensional instability growth. $\alpha_i$ is the non-dimensionalized spatial amplification rate.

The experimentally determined quantity to be compared with this result is the fringe (i.e. the isotherm) displacement amplitude. The disturbance temperature amplitude $\theta$ at a point is related to the isotherm displacement amplitude $D$ at that point by

$$\theta/D = \partial T/\partial y, \tag{6}$$

where $\partial T/\partial y$ is the dimensional gradient of the base flow temperature. Since the experimental results consist of $D$ as a function of $x$ along an isotherm, the theoretical disturbance temperature amplitude growth, i.e (5), must be corrected for the change of the base flow temperature gradient $\partial T/\partial y$ along the isotherm. In the boundary layer this dimensional gradient is proportional to the non-dimensional gradient $T'(\eta)$, where $\eta = y/\delta_c$. Based on the total fringe shift at the foil and the theoretical foil temperature, the temperature of the fifth fringe was determined at two locations ($x = 3$ in. and 6 in.). The two temperature determinations agreed to within less than 1 %. The value of the dimensionless temperature was determined at several intermediate locations by dividing the temperature corresponding to the fifth fringe by $T_c$ at each location. The value of $T'$ was determined at each location along the fringe from a plot (theoretical) of $T(\eta)$ *versus* $T'(\eta)$. From this result it was shown that

$$T'(\eta) \propto x^{-0{\cdot}12} \propto G^{*-0{\cdot}15}. \tag{7}$$

This exponential is a good approximation to the dependence of $T'$ on $x$ (or $G^*$) along the fifth fringe. When combined with (5) this gives the factor $G^*/200$ a power of 0·40.

The temperature disturbance amplitude, and displacement amplitude, growth calculated from theory have been plotted *versus* $x$ for frequencies of 0·12 and 0·25 Hz. The first frequency corresponds to the most amplified path for disturbances introduced at the vibrator location (i.e. $1\frac{1}{2}$ in. from the leading edge at $G^* = 91{\cdot}73$). The results are shown as the theory curves in figure 8. Two curves are shown for each frequency; one is the temperature amplitude and the other is the isotherm displacement amplitude. These correspond to powers of $x$ of 0·20 and 0·32 (0·20 + 0·12) for the two cases respectively. The theoretical results are presented in this manner to facilitate a direct comparison with the experimental data. The 0·25 Hz disturbance crosses the neutral curve at $x = 2{\cdot}01$ in., as indicated in figure 8. The slope of the temperature amplitude and the isotherm displacement amplitude curves at this location are 0·20 and 0·32 respectively because of the growth of the characteristic temperature ($T_c \propto x^{0{\cdot}20}$) and the reduction of the base flow temperature gradient ($T' \propto x^{-0{\cdot}12}$) along the fifth fringe.

The experimental data obtained from the *moiré* patterns is in generally good agreement with the theoretical results. The difference in amplification for the two different frequencies is significantly greater than the spread in the data at each frequency. The data were found to be in better agreement with the displacement amplitude curves than with the disturbance temperature amplitude curves

*Disturbance behaviour at low frequencies*

At frequencies below 0·1 Hz, higher harmonics can be seen in the anemometer output, figure 9. These higher harmonics become increasingly dominant as the input frequency is reduced. At the lowest frequency examined (0·05 Hz), the higher harmonic is almost as strong as the input frequency. At 0·10 Hz the disturbances appear to contain only the input frequency. In this study the vibrator was at $x = 1\frac{1}{2}$ in. and the anemometer probe was at $x = 6\frac{1}{2}$ in. Because of the low frequencies and the resulting long wavelengths, interferograms did not show this behaviour clearly.

There is no guarantee that the disturbance wave-form in the fluid is precisely the same as the vibrator displacement wave-form. Thus it is impossible to say whether the higher harmonics are contained in the vibrator motion, whether they are generated in the coupling between this motion and the fluid motion, or whether they are generated from an initially pure fluid disturbance, i.e. one with no higher harmonics present. Regardless of the source of these higher harmonics, the reason for their dominance can be seen in figures 1 and 2 of Dring & Gebhart (1968). At these low frequencies the higher harmonics amplify much faster than the base frequency. For an input of 0·06 Hz, the relative amplification for the higher harmonic (0·12 Hz) is about twice that of the base frequency. This relative difference in amplification becomes greater for lower input frequencies.

The paths $f_1$ and $f_2$ (in Dring & Gebhart (1968), figures 1 and 2) correspond to frequencies of about 0·02 and 0·11 Hz respectively (at a foil current of 1 amp). $f_2$ is the most amplified path from the neutral curve up to $G^* = 300$. $f_1$ is the curve

that begins to amplify first (at the critical $G^*$). The higher harmonics are most likely to dominate disturbances on path $f_1$ but the base frequency should dominate on path $f_2$.

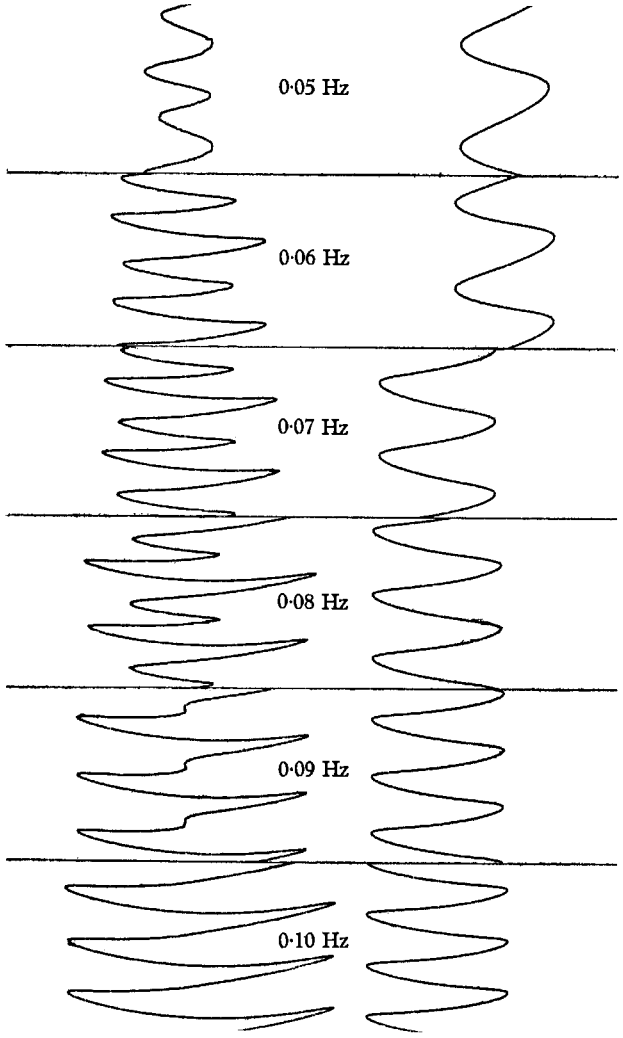


FIGURE 9. Recordings of higher harmonics. Right trace: vibrator input; left trace: anemometer output (at $6\frac{1}{2}$ in.).

## 4. Conclusions

Past experimental studies of natural convection instability have generally lacked either accurate calibrations for the measurement of the disturbance velocity, or theoretical results suitable for direct comparison, or both. Colak-Antic (1964) measured disturbance velocities, but the accuracy is uncertain owing to the effects of the coupling of the relatively large temperature disturbances with velocity in the output of the hot-wire anemometer. The small temperature differences and the calibration of the hot-wire anemometers (appendix A) made

possible a direct comparison between the experimental data of the present work and the theoretical results of Dring & Gebhart (1968) over the entire range of location and disturbance frequency.

The experimental results of the present work are in excellent and detailed agreement with the linear disturbance theory. The theoretical amplitude and phase profiles have been compared with the experimental profiles. The comparison was made with both hot-wire anemometer data on the disturbance velocity profiles and with interferometric data on the disturbance temperature profiles. Good agreement is found with theory with both types of experimental investigation. Experimental disturbance profiles are slightly thinner than the theoretical profiles. The general profile shapes, however, bear many clear similarities. The theoretical and experimental results are in good agreement about the changes in the profile shapes as a disturbance is convected downstream.

Theory predictions of amplification rate and disturbance amplitude growth have also been compared with the experimental results. The spatial amplification rate has been measured from the growth of disturbance velocity amplitude with a hot-wire anemometer. This amplification rate has been measured as a function of frequency. The theoretical prediction is well within the error band of the experimental results. The growth of a disturbance in the temperature field as it is convected downstream has been measured interferometrically. The measurements at two frequencies examined are in good agreement with the predictions.

The importance conventionally ascribed to the critical $G^*$ is diminished for the flows considered here because the low-frequency disturbances associated with the critical $G^*$ region are well below the most amplified frequency and are dominated downstream by higher harmonics. The source of these higher harmonics in this study is uncertain, but they have been found to become increasingly important as the input frequency is lowered below the most amplified value.

Some additional supporting results can be found in the work of other authors. Colak-Antic (1964) calculated the maximum amplification rate in his flow based on hot-wire measurements. In the notation of the present work, his measurement corresponds to $\alpha_i = -0{\cdot}051$. The uncertainty in his result is listed as $\pm 170\,\%$, but this is probably a printing error. This maximum amplification rate is in good agreement with the value determined theoretically by Dring & Gebhart (1968), namely $-0{\cdot}055$. This comparison is interesting, but it should not be given too much importance because of the significant differences between the theoretical and the experimental flows.

Knowles (1967) has presented some data on the appearance of amplified 'natural' disturbances in a flow which is identical with that investigated in the present work. These data are shown in figure 10 along with some of the theoretical results of Dring & Gebhart (1968). The neutral curve $\alpha_i = 0, 1{\cdot}0x$, two amplification rate contours $\alpha_i = -0{\cdot}025$ and $-0{\cdot}05475$ and two amplitude ratio contours $10x$ and $20x$ are shown. Four constant-frequency paths are also indicated. It can be seen that $f_2$ is about 5·4 times greater than $f_1$. It can also be seen in the theoretical results that the most amplified frequencies for values of $G^*$ greater than 300 will be greater than the most amplified frequency for 300. The naturally occurring disturbances presented by Knowles (1967) are in a band between the most

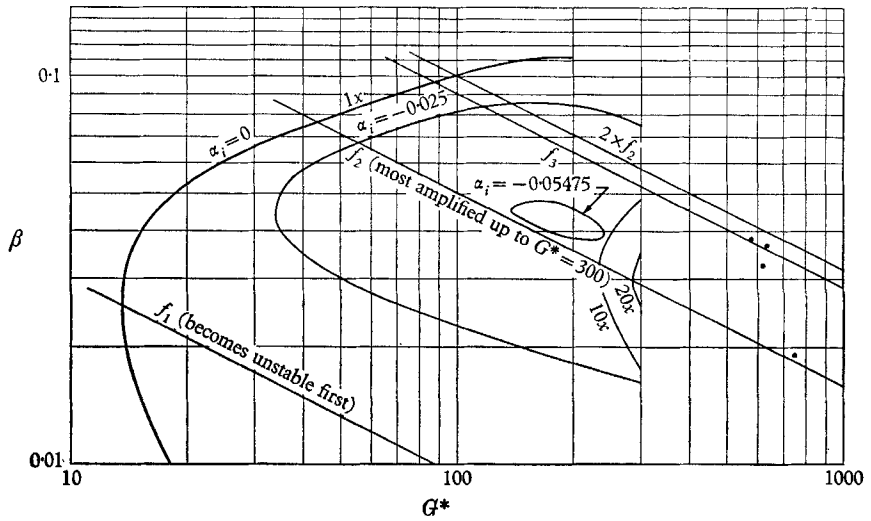


FIGURE 10. The stability plane ($\beta$ *versus* $G^*$). •, natural oscillations recorded by Knowles (1967).

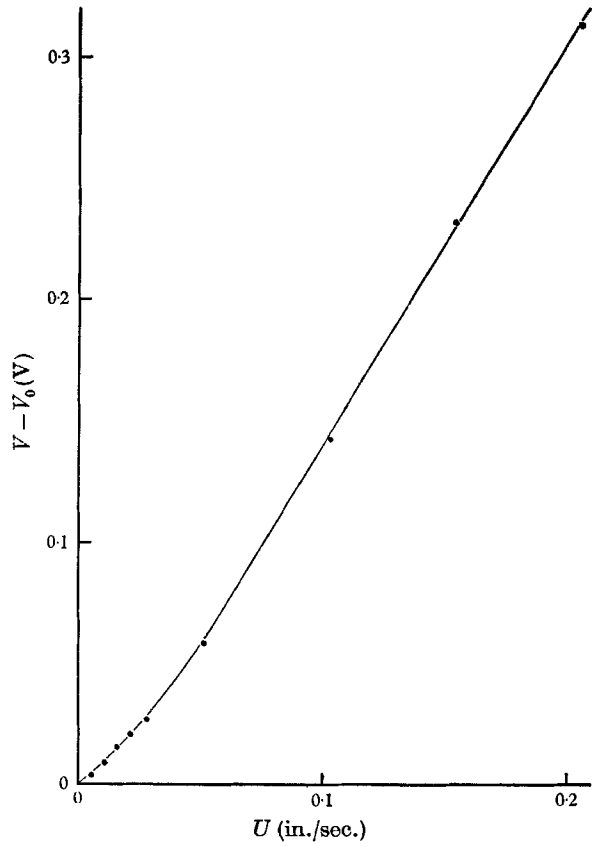


FIGURE 11. Hot-wire anemometer calibration (resistance ratio = 1·3).

amplified frequency at $G^* = 300$ ($f_2$) and twice that frequency ($2 \times f_2$). This clearly supports the hypothesis that natural disturbances arise out of the most amplified frequencies, rather than the frequency which begins to amplify first.

The authors wish to acknowledge the support of the National Science Foundation through grants GP-127 and GK-1963 for this research. They would also like to thank Dr C. P. Knowles and Prof. S. F. Shen for their suggestions and advice.

## Appendix A

The hot-wire anemometers (constant-temperature type) were calibrated over the range of velocities expected in the natural convection velocity profile. The results are shown in figure 11. The lowest velocity considered was 0·0051 in./sec. The calibration was achieved by raising a container of the test fluid while the probe was held stationary in the fluid. This flow arrangement was chosen so as to be as close as possible to the experimental situation of the fluid rising past the stationary probe. The apparatus is described in detail by Dring (1968).

The anemometer output was presented in the form of the difference between a time-average anemometer voltage ouput with the fluid in motion $V$ minus the voltage output with the fluid held stationary $V_0$. $V_0$ was taken as the average of the output before and after the test. If these initial and final voltages were significantly different, i.e. relative to $V - V_0$, the data point was rejected. The fluid velocity was determined by timing the distance interval over which the time-average voltage $V$ was determined.

As can be seen in figure 11 the calibration curve is nearly linear over a wide range at higher velocities. For this reason, the anemometer output could be taken as nearly proportional to the velocity input. There are, however, several differences between the calibration and experimental flows. The probes were calibrated in a time-steady, uniform stream at constant temperature. The experimental flow, however, is an unsteady (oscillating) shear flow with an oscillating temperature field. These effects have been ignored since they are expected to be relatively weak. It would be a separate and very difficult study to include these effects in the calibration.

## REFERENCES

Colak-Antic, P. 1964 *Jahrbuch der WGLR*, 172.
Dring, R. P. 1968 Ph.D. Thesis, Cornell University.
Dring, R. P. & Gebhart, B. 1968 *J. Fluid Mech.* **34**, 551.
Gebhart, B. &. Knowles, C. P. 1966 *Rev. Scient. Instrum.* **37**, 12.
Knowles, C. P. 1967 Ph.D. Thesis, Cornell University.
Knowles, C. P. & Gebhart, B. 1968 *J. Fluid Mech.* **34**, 657.
Nachtsheim, P. R. 1963 *NASA* TN D-2089.
Polymeropoulos, C. E. 1966 Ph.D. Thesis, Cornell University.
Polymeropoulos, C. E. & Gebhart, B. 1966 *AIAA J.* **4**, 2066.
Polymeropoulos, C. E. & Gebhart, B. 1968 *J. Fluid Mech.* **30**, 225.
Schubauer, G. B. & Skramstad, H. K. 1948 *NACA* Rep. no. 909.

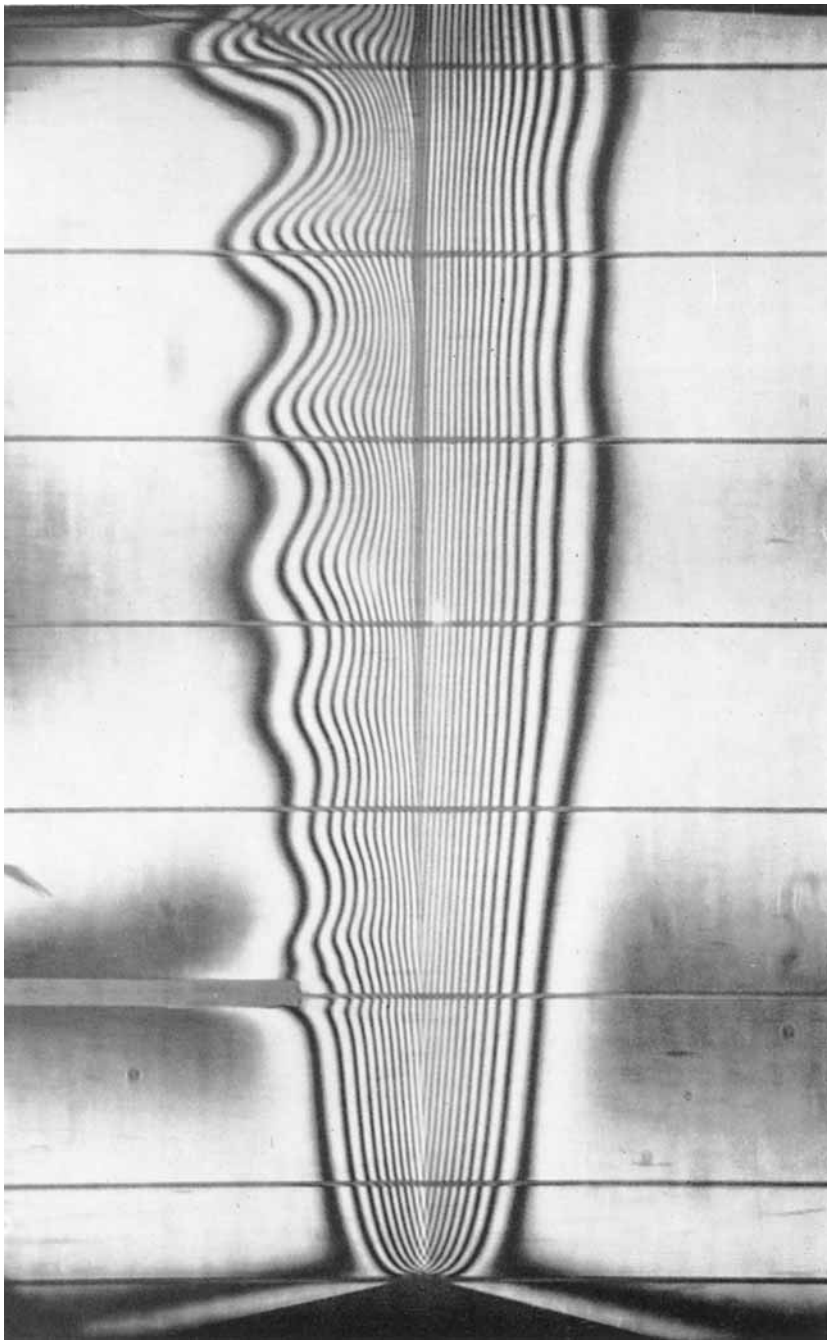

FIGURE 5. Infinite fringe interferogram at 0·20 Hz.

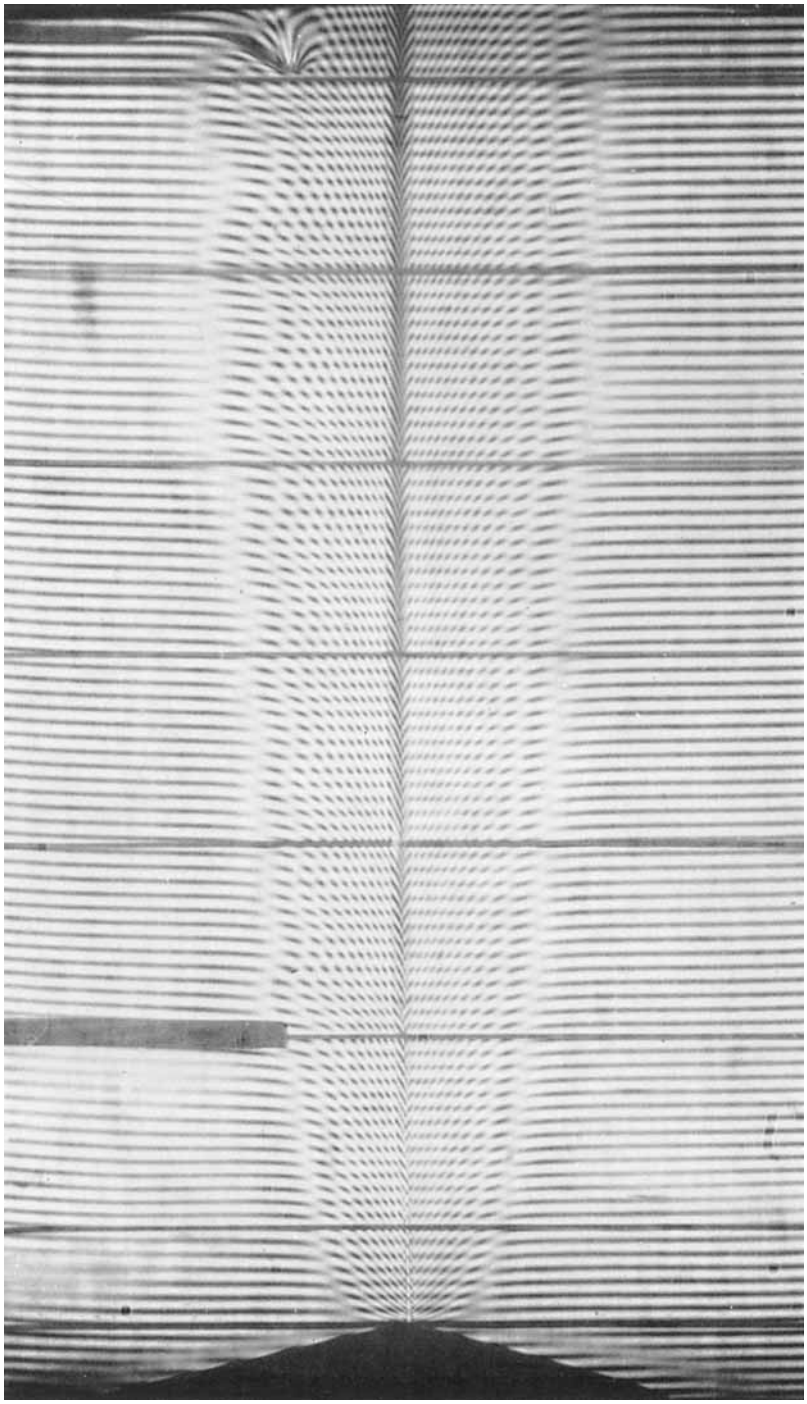

FIGURE 7. Finite fringe interferogram (*moiré* pattern) at 0·25 Hz.